Mathematical and Computer Modelling 57 (2013) 1312–1324

Contents lists available at SciVerse ScienceDirect

Mathematical and Computer Modelling

journal homepage: www.elsevier.com/locate/mcm

Computational modelling of the embolization process for the treatment of arteriovenous malformations (AVMs)

A.H. White *, F.T. Smith

Department of Mathematics, University College London, Gower Street, London, WC1E 6BT, United Kingdom

ARTICLE INFO

Article history:
Received 22 August 2011
Received in revised form 18 October 2012
Accepted 28 October 2012

Keywords:
Arteriovenous malformation
Embolization
Branching
Multiphase
Volume of fluid

ABSTRACT

Arteriovenous malformations (AVMs) are neurological defects in which the arterial and venous systems are connected directly, with no intervening capillaries. The absence of capillaries allows blood at high pressure to enter the venous system directly, and so a venous haemorrhage or a stroke is possible. AVMs can be treated by embolization in which a glue is injected into a local artery with the aim of diverting the blood away from the AVM and so reducing the risk of haemorrhage. The present study introduces a novel mathematical model for the embolization procedure by considering a two-phase fluid dynamical approach for the glue/blood interaction. The two fluids are treated as incompressible and viscous, and their interaction is modelled using the volume-of-fluid method, with the aim of analysing the dynamics of the glue after injection and examining potential blocking strategies. The results obtained here include surface tension effects and point to advantageous placement, blocking and effective solidification in particular.

1. Arteriovenous malformations and endovascular embolization

Arteriovenous malformations (AVMs) can be categorized as defects of the circulatory system, which are generally thought to be congenital (present at birth or early in life and slowly developing over time): in fact usually no specific cause for the AVM can be identified. Although AVMs can occur in many different areas of the human body, not just in the brain, the current concern is with cerebral AVMs because of the health consequences and their ability to lead to a mortality. In an AVM, blood at high pressure in the arterial system empties directly into the venous system (which is at low pressure) due to the absence of intermediate capillaries. Veins have only very thin walls however, and they are capable of containing blood at relatively low pressure only. The abnormally high flow rate causes the blood pressure to rise to dangerously high levels, and there is then a distinct possibility that the wall of the vein may break due to the high pressure, causing a venous haemorrhage. Cerebral AVMs occur in approximately 10 out of 100 000 people [1] and are slightly more common in males. Although the lesion is often present at the time of birth, symptoms may occur at any time and often present themselves when the patient is aged between 20 and 40. Typical symptoms of AVMs include severe headache, weakness and paralysis, and even hallucinations or dementia.

An AVM poses a complicated clinical problem. The clinician must determine the best strategy for treating or removing the malformation without causing a haemorrhage, a challenge which can be difficult due to abnormally weak blood vessels. Administration of drugs may help to overcome the earlier-described symptoms that are associated with AVMs, but the main aim is either to remove or to alter the lesion. There are currently three primary techniques used to do this: conventional neurosurgery, endovascular embolization, and radio-surgery. The choice of technique is dependent on both the size and the

* Corresponding author.
E-mail address: alexw@math.ucl.ac.uk (A.H. White).

0895-7177/$ – see front matter
doi:10.1016/j.mcm.2012.10.033

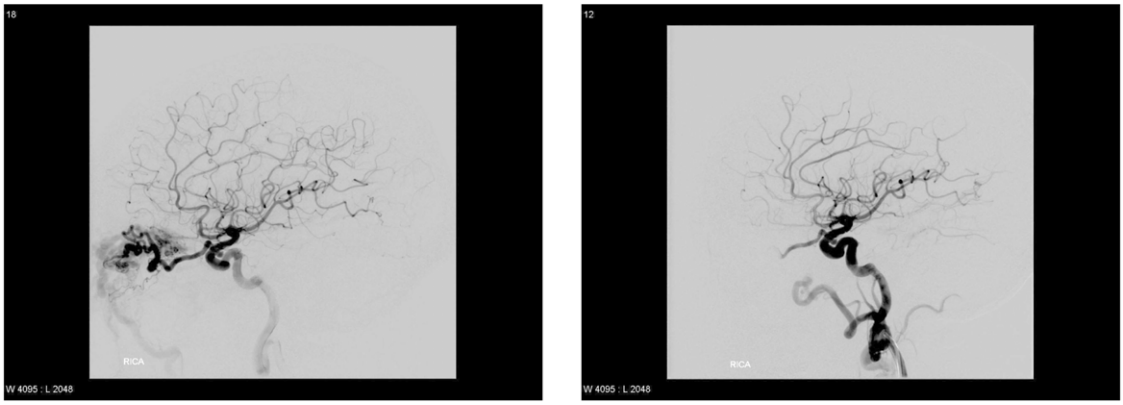

Fig. 1. Two angiograms showing the blood flow when the AVM is present (left) and after treatment with embolization (right).

position of the AVM. Only complete obliteration of the AVM is a definitive cure, and this is possible only in a relatively small number of cases.

In an AVM there is a reduced vascular resistance, and hence an increased flow rate occurs from the arterial to the venous system. The two main surgical procedures used as mentioned earlier are clipping and glue-casting, to reduce the mass flux through the AVM. Owing to the limited understanding of these procedures and their outcomes, these procedures tend to err on the side of caution. The embolization procedure is described in the subsection immediately below, followed by discussions of models and the present approach.

1.1. The embolization process

Embolization is one of the most common procedures in the treatment of AVMs, and it has the clear advantage of being less invasive than forms of conventional neurosurgery. The technique was pioneered in the early 1960s by Lussenhop [2]. With improved technology and understanding, it is now possible to reach and successfully embolize quite complex AVMs in functional-dependent areas of the brain. Embolization may be performed as the sole treatment for an AVM or it may be combined with radio-surgery or conventional neurosurgery, and indeed patients having the latter treatments usually require embolization first anyway if the lesion is larger than 3 cm across.

Embolization is almost always given to a patient under general anaesthetic. A small catheter is inserted into a blood vessel, typically the femoral artery in the thigh, and then passed along the network of blood vessels to the feeding artery of the AVM, using X-ray guidance of the catheter. Sometimes a very fine micro guide wire is used to achieve optimum positioning of the catheter. A glue is then passed through the catheter into the AVM, with the tip of the catheter being positioned as close as possible to the branching site of the AVM. The aim of the procedure is to make the glue occlude the abnormal blood vessels so that blood is no longer able to flow through the malformation. This is illustrated in Fig. 1, which shows an angiogram of an AVM before and after the embolization process. When there is no longer any blood passing through an AVM, there should be no further risk of bleeding. For larger AVMs, embolization is often done in stages such that at each stage a certain section of the AVM is blocked off. The glue that is used is initially in a liquid state in order to penetrate small vessels, and then it hardens on contact with ions such as those present in the blood.

Sometimes more than one embolization is needed, as just stated, particularly when the AVM is comparatively large, and also for the sake of avoiding too rapid or drastic alterations of the blood flow patterns in the brain. It should be noted that even though the embolization procedure may have been carried out successfully the blood vessels may open again over time as the body tries to remove a foreign material such as the glue. If this occurs, the procedure can be repeated, or another type of treatment may then prove more beneficial.

1.2. Models

There has been a considerable amount of research dedicated to the modelling of blood flow in arteries, as for example [3–6], but much less on the haemodynamics associated with AVMs. Some models have aimed to simulate the flow in a simplified geometric configuration where the model is made up of a multiple array of parallel compartmentalized vessels [7]. Another type of model for AVMs uses electrical circuit analysis [8], which aims to relate flow pressures to volume fluxes in networks, primarily with the desire to explain steal phenomena. Here, ‘steal’ refers to strong throughput in the AVM which weakens cerebral throughput elsewhere.

Typically an AVM has many feeding arteries, each one of which may branch into as many as 50 daughters and granddaughters. Attempts have been made to analyse the flow structure in both the mother and the daughters: see [9–12]. The first of these considers a linear problem of a flow at high Reynolds number through a branching geometry, in both two- and three-dimensional settings. The role of the geometrical structure as well as the mass flux in the daughters is analysed for

multiple small daughters. The work in [11] on the other hand gives a nonlinear analysis of the flow assuming that the fluid is inviscid; this is justified in some contexts by the fact that the boundary layer thickness is nominally small compared to the thickness of the vessel downstream. The model analyses flow over short length scales, finds recurrence relations between the flow profiles in each of the daughters, and then solves the recurrence relations numerically and analytically. The model is useful because it is able to deal with branchings that produce considerably less solid area downstream, and hence more realistic geometries may be applied to this model. Fully three-dimensional effects of flow from one mother to two daughters have also been studied [13–15]. In [14], a purely numerical finite-volume simulation is compared to slender flow analysis where the streamwise length scale is of order of the Reynolds number and strictly larger than the two cross-sectional length scales. Results for the wall shear and pressure as well as the velocity profiles are obtained in cases of one mother branching to two daughters, and close agreement is found between the theory and the numerical computations.

Recently, lattice Boltzmann methods have been used to model AVMs [16,17]. These methods use a combination of ideas from statistical mechanics and cellular automata to model the flow in complicated geometries. Lattice Boltzmann methods aim to simulate macroscopic flow conditions by considering the statistical distribution of particles representing the microscopic fluid flow. This method is becoming ever more popular and appears to be potentially very useful for modelling AVMs and their accompanying complicated geometry.

1.3. The present approach

It is intended that the present work will set up a basic mathematical model for the embolization process. Comparatively little modelling of this kind has been done in the application area previously, to the best of our knowledge, and so the approach is seen rather as a first step in modelling such a complex procedure in two spatial dimensions. Although some of the simplifications made in the present work may oversimplify the complex chemical processes at work here, it is hoped this can be incorporated into further studies on the subject. Factors such as solidifaction, polymerization, three-dimensional effects, and the non-Newtonian properties of the glue and the blood will be studied in future work. Section 2 below describes the general model in appropriate detail, leading to the equations of motion and boundary conditions, along with the solution methodology which is based on a volume-of-fluid approach. This is followed by Section 3 addressing a specific branching-channel-flow model, with computational results and then potential blocking strategies being explored, while Section 4 examines the effects due to surface tension. Section 5 provides final comments on the study.

2. Mathematical model and equations of motion

The combined motion of two fluids in a multi-branching channel is considered with the walls of all the vessels involved being fixed, similarly to the arrangements in [10,11]. Models of motion of a single fluid through a branched network with moving walls can be found in [18,19] for comparison. The dimensional coordinates are given by x^* and y^*, denoting distance along the channel wall and perpendicular to it respectively. The pressure is denoted by p^* and the interface between the glue and blood is denoted $y^* = f(x^*, t)$. For the current relatively simple start-up model, we consider the case where both fluids (the blood and glue) are incompressible Newtonian fluids. This should be quite an accurate assumption for the blood, taking into account the size of the containing vessels considered here, but is it probably a rather more naive assumption for the glue.

The diameter of the feeding artery is taken to be in the range $l^* = 0.001$ to 0.005 m, with the typical streamwise velocities of blood flow in AVMs being as high as $U^* = 1.3$–$1.5\ \mathrm{ms}^{-1}$ [20]. The density for the commonly used glue N-butyl-2-cyanoacrylate (Histoactyl) is $1.44\ \mathrm{g/cm}^3$, while that of the added radio-opaque oil, Lipiodol, is given as $1.280\ \mathrm{g/cm}^3$. Typically the injected mixture consists of 80% Lipiodol and 20% N-butyl-2-cyanoacrylate, giving an overall density of approximately $1.32\ \mathrm{g/cm}^3$. This density is comparable to the density of blood, which is taken to be $1.063\ \mathrm{g/cm}^3$, and so in the model we may fix the density ratio to be unity at a first approximation. Taking the kinematic viscosity of blood to be $\nu = 4.78 \times 10^{-6}\ \mathrm{m}^2\mathrm{s}^{-1}$, we find that the Reynolds number $Re = U^* l^*/\nu$ for a typical flow in this setting ranges between 280 and 1500. Biomedical flows of this type are very rarely turbulent even at such high relatively high Reynolds numbers, and in consequence all of the modelling described in the present paper assumes laminar flow. Effects of the outer wall shape on the multiphase flow similar to that considered here are introduced in a related study by [21].

2.1. The model equations and conditions

Throughout, all quantities associated with the glue are represented with subscript 1 and those associated with the blood with subscript 2. The velocity fields of the respective fluids are given by $\mathbf{u}_i^* = (u_i^*, v_i^*)$, with corresponding density and pressure fields ρ_i^* and p_i^*, with $i = 1, 2$, while the non-dimensional variables for the model are given by $(u_i, v_i, p, t) = (u_i^*/U, v_i^*/U, p^*/U^2\rho_2, t^*U/l)$. The non-dimensional coordinates are $x = x^*/l$ and $y = y^*/l$, measuring distance along the channel wall and perpendicular to it, respectively. The governing equations in each fluid are thus the non-dimensional incompressible Navier–Stokes and continuity equations:

$$\frac{\partial \mathbf{u}_1}{\partial t} + (\mathbf{u}_1 \cdot \nabla)\,\mathbf{u}_1 = -\left(\frac{\rho_2}{\rho_1}\right)\nabla p_1 + \left(\frac{\nu_1}{\nu_2}\right)\frac{1}{\mathrm{Re}}\nabla^2\mathbf{u}_1, \quad \nabla \cdot \mathbf{u}_1 = 0; \tag{1}$$

$$\frac{\partial \mathbf{u}_2}{\partial t} + (\mathbf{u}_2 \cdot \nabla)\,\mathbf{u}_2 = -\nabla p_2 + \frac{1}{\mathrm{Re}}\nabla^2 \mathbf{u}_2\,, \quad \nabla \cdot \mathbf{u}_2 = 0. \tag{2}$$

In addition to the no-slip conditions applying at the containing walls, the equations are complemented by conditions holding at the unknown interface between the glue and the blood. These are made up of the kinematic condition, the continuity of normal and tangential stress, and the continuity of velocity at the unknown interface $y = f(x, t)$. The kinematic condition,

$$\frac{\partial F}{\partial t} + \mathbf{u}_i \cdot \nabla F = 0, \tag{3}$$

where $F = y - f(x, t)$, effectively states that a fluid particle on the interface must remain on the interface and is advected with the local velocity field $\mathbf{u}_i$. The condition that the components of velocity normal to the interface are equal in each fluid is written as

$$\mathbf{u}_1 \cdot \mathbf{n} = \mathbf{u}_2 \cdot \mathbf{n}, \tag{4}$$

where $\mathbf{n}$ is the outward-pointing normal to the interface; the corresponding tangent vector $\mathbf{t}$, defined at an angle of $\pi/2$ clockwise from the given normal vector, will also be utilized below. The dynamic condition at the interface is obtained by applying a momentum balance to a volume element at the interface. This balance gives

$$-p_1\mathbf{I} + 2\mu_1\mathbf{D}_1 \cdot \mathbf{n} = -p_2\mathbf{I} + 2\mu_2\mathbf{D}_2 \cdot \mathbf{n}, \tag{5}$$

where the stress tensor $\mathbf{D}$ is given by $(\partial_i u_j + \partial_j u_i)/2$ in each fluid (see [22]) and $\mathbf{I}$ is the identity tensor. Forces such as surface tension have been ignored for now, but the effects from surface tension will be studied anew in Section 4. The continuity of tangential stress dictates that

$$\mu_1 \mathbf{t} \cdot \mathbf{D}_1 \cdot \mathbf{n} = \mu_2 \mathbf{t} \cdot \mathbf{D}_2 \cdot \mathbf{n}. \tag{6}$$

Next, a brief outline of the solution procedure for the system (1)–(6) is given.

2.2. General outline of the method

We implemented the open-source Gerris flow solver (http://gfs.sourceforge.net) to solve the multiphase system. Gerris solves the time-dependent incompressible Euler or Navier–Stokes equations on a quadtree adaptive mesh in two-dimensional mode as used in this study, although the solver also has the capacity to deal with three-dimensional flows. The well-known volume-of-fluid (VoF) method is used to track the interface [23]. We now outline the main steps of the VoF algorithm in Gerris. An indicator or colour function $C(\mathbf{x}, t)$ is defined to track which phase occupies different grid cell(s) in the computational domain: in our case this amounts to requiring $C = 1$ in the blood and $C = 0$ in the glue. The colour function satisfies the advection equation

$$\partial_t C + \mathbf{u} \cdot \nabla C = 0, \tag{7}$$

which is essentially the analogue of the kinematic condition (3), with $\mathbf{u}$ being the interfacial velocity.

There are three main ingredients of the volume-of-fluid method. These are firstly advecting the interface, secondly reconstructing the interface from a specific colour function field, and thirdly solving the governing Navier–Stokes equations. The advection amounts to solving (7) and is carried out using a Lagrangian method to find updated values of the colour function. Next, the interface is reconstructed, details of the method being found in [24], while extensions are presented in [25]. The governing equations are solved in the so-called 'one-fluid mode' [26]. Here, the two momentum equations (1) and (2) are replaced by a single momentum equation with variable viscosity and density which applies throughout the computational domain,

$$\frac{\partial \mathbf{u}}{\partial t} + (\mathbf{u} \cdot \nabla)\,\mathbf{u} = -\frac{1}{\rho}\,\nabla p + \frac{1}{\rho}\frac{1}{\mathrm{Re}}\nabla \cdot (2\mu\mathbf{D}). \tag{8}$$

Note here that the factor μ is now present inside the divergence operator. This is due to the fact that in the one-fluid formulation the value of μ defined below is no longer constant across the interface. Now, the values of density and kinematic viscosity are given respectively by $\rho = C\rho_1/\rho_2 + (1-C)$ and $\mu = C\mu_2/\mu_1 + (1-C)$. The well-known projection method [27] is used to solve the Navier–Stokes equations; full details can be found in [28]. This is essentially a fractional-step method in which an intermediate velocity field is projected onto the space of divergence-free fields, yielding a Poisson equation for pressure, when combined with the continuity equation. The main stages of the algorithm are listed below. First, the intermediate velocity $\tilde{u}$ is calculated from the discretized Navier–Stokes equations without the pressure gradient term:

$$\frac{\tilde{\mathbf{u}} - \mathbf{u}^{(n)}}{\Delta t} = -\mathbf{u}^{(n+1/2)} \cdot \nabla \mathbf{u}^{(n+1/2)} + \frac{1}{\mathrm{Re}\rho^{(n)}}\nabla \cdot \left[\mu^{(n)}(\mathbf{D}^{(n)} + \tilde{\mathbf{D}})\right]. \tag{9}$$

Here, the superscript n refers to evaluation at the nth time step, while those variables with tildes are evaluated at the $(n + 1/2)$th intermediate time step. The advection terms are discretized using the second-order Godunov unsplit upwind

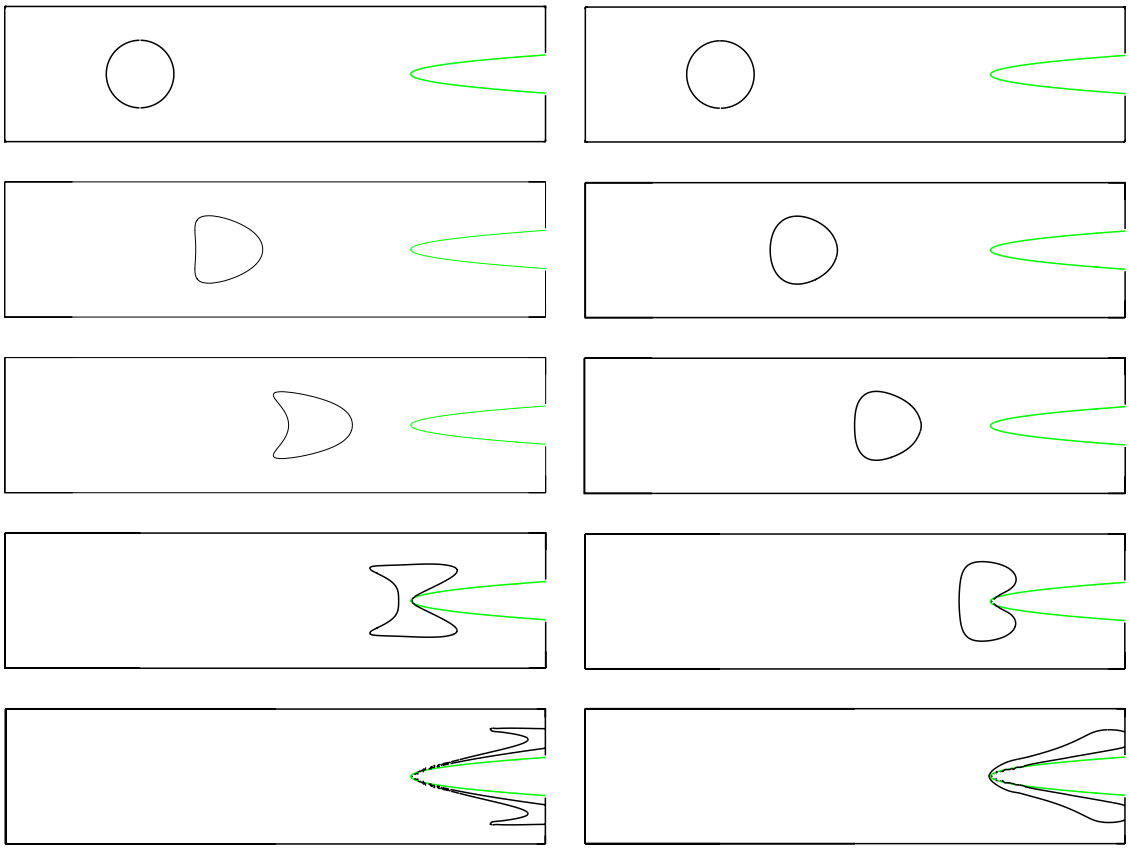

Fig. 2. Interface positions for the flow of an initially circular glue droplet, at $Re = 400$, from a single mother to two daughters. Plots shown are for $\nu = 1$ (left) and $\nu = 10$ (right), for non-dimensional times of 0, 5, 10, 15, and 20, from top to bottom.

method of [29], whereas a second-order Crank–Nicholson routine is used for the diffusive term. Using (9), an equation for the velocity at the next time step can then be found:

$$\frac{\mathbf{u}^{(n+1)} - \tilde{\mathbf{u}}}{\Delta t} = -\frac{1}{\rho^{(n)}} \nabla p^{(n+1)}. \tag{10}$$

Since the velocity field must be divergence free,

$$\nabla \cdot \tilde{\mathbf{u}} = \Delta t \nabla \cdot \left(\frac{1}{\rho^{(n)}} \nabla p^{(n+1)} \right). \tag{11}$$

This equation is solved with a multi-grid method to determine the pressure field, which then gives the velocity field from (10).

3. A simple channel flow model and results

In the present very simple model, the glue is assumed to be injected in a single mother vessel upstream. The resulting flow into two or more daughter vessels downstream and the flow interactions between the mother and daughter vessels are then analysed. In practice, the glue must be injected into the feeding artery, since generally the vessel (daughter vessel) that needs to be blocked is too small for the catheter. Another practical reason for injecting in the mother vessel is the reduced chance of an embolic stroke occurring. Mathematically, it is taken that the glue is injected as a droplet rather than a continuous stream as is usually the case in practice [30]. Studies of droplet dynamics in different applications are widespread and can be found in the fields of aircraft icing, ink-jet printing, atomization, and many others. Moreover, studies of droplet flows in microfluidics are common [31,32]. The former paper here uses the Gerris flow solver to analyse the dynamics of droplets in T-junctions. The predictions for the flow of a droplet within another fluid from one mother to two symmetric daughters can be found in [33], where conditions for droplet splitting based on the global capillary number are found. Numerical solutions for the inviscid flow of two fluids in channels are given in [34,21]. The present study concentrates on flow from a single mother vessel to daughter vessels; no modelling of the flow to grand-daughters is attempted, although this would be a

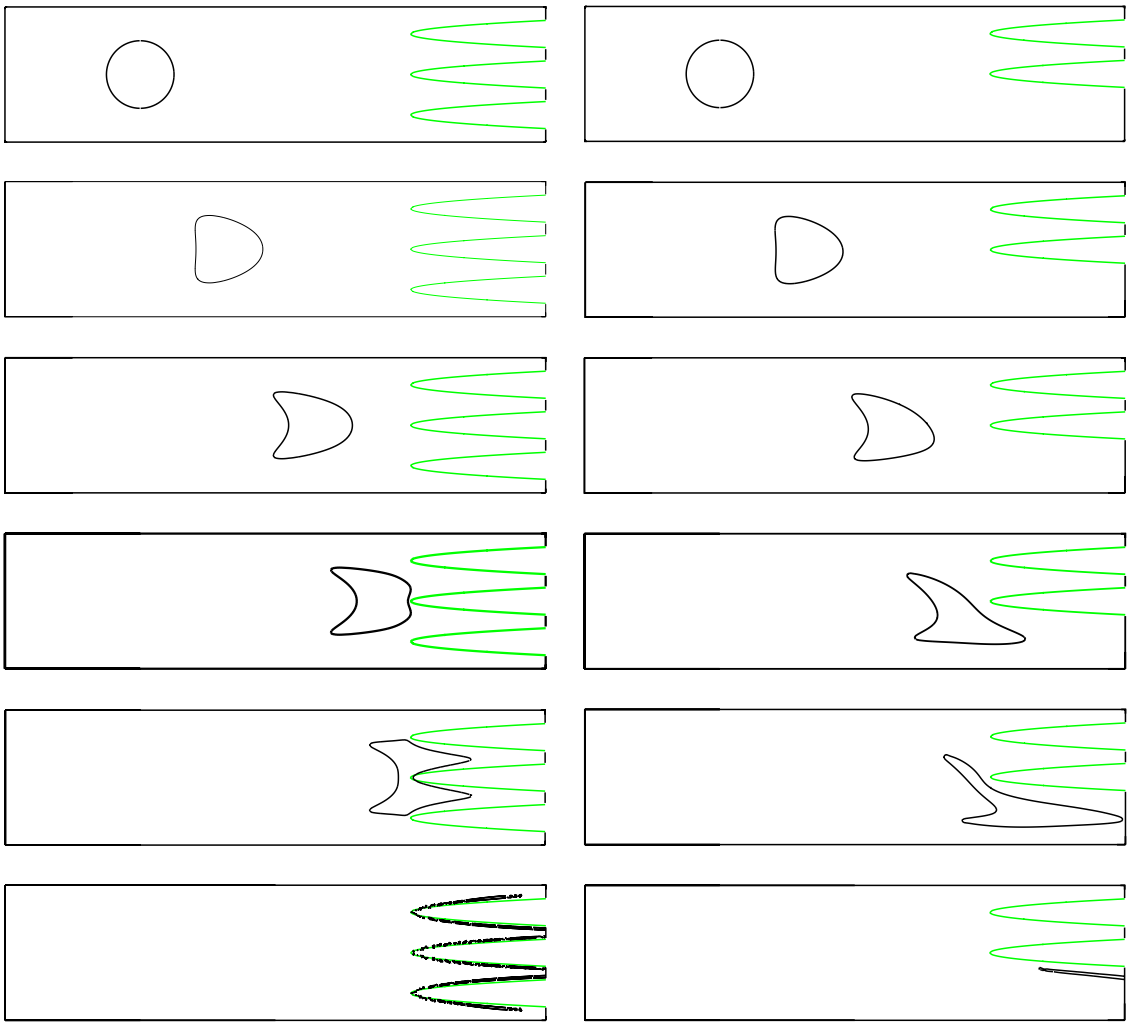

Fig. 3. Interface positions for the flow of an initially circular glue droplet from a single mother to four symmetric daughters (left) and to three non-symmetric daughters (right). Shown from top to bottom at non-dimensional times of 0, 5, 10, 12.5, 15, and 20.

simple extension of the current model in principle. Situations such as those above are described in [17,35] for a single fluid, with the former study attempting analytical and numerical approaches while the latter is a purely numerical treatment using a network model.

In all of the present computations the Reynolds number Re is fixed as 400, which is within the realistic range stated earlier. Results with larger Reynolds numbers, but still within the range quoted earlier, give similar qualitative results. For instance, considering flows at higher Reynolds numbers, the glue droplet enters the daughter at earlier non-dimensional times, and there is less distortion to the upstream section of the interface shape. The work here examines the channel flow in a number of geometrical settings, although the dynamics near the branching of the daughter vessels is of prime importance. The geometrical settings are relatively basic, comprising an incident channel with rigid walls and various combinations of daughter vessel shapes modelled as solid parabolas downstream of the branch junctions. The domain is fixed as $0 \leq x \leq 4$ and $0 \leq y \leq 1$, and there are $2^{11} \times 2^9$ grid cells in the respective dimensions. The adaptive mesh refinement used is based on the vorticity field as well as the gradient of the interface and the solid boundaries. The inflow velocity is set to be the fully developed Poiseuille form $u = y(1 - y)$, while no-slip conditions are applied at the upper and lower walls as well as the daughter walls. On the right-hand side of the domain standard outflow conditions are set, with Neumann conditions imposed on all boundaries for the colour function. In most realistic cases the glue and the blood are of comparable density, as mentioned earlier, and so the focus below is on cases where $\rho_1 = \rho_2$.

3.1. Basic results

Fig. 2 shows the interface positions for the glue droplet at non-dimensional times of $t = 0, 5, 10, 15$, and 20. Here the droplet is initially circular with a radius of 0.2 and its centre is at $y = 0.5$. The two cases shown, both being from one mother

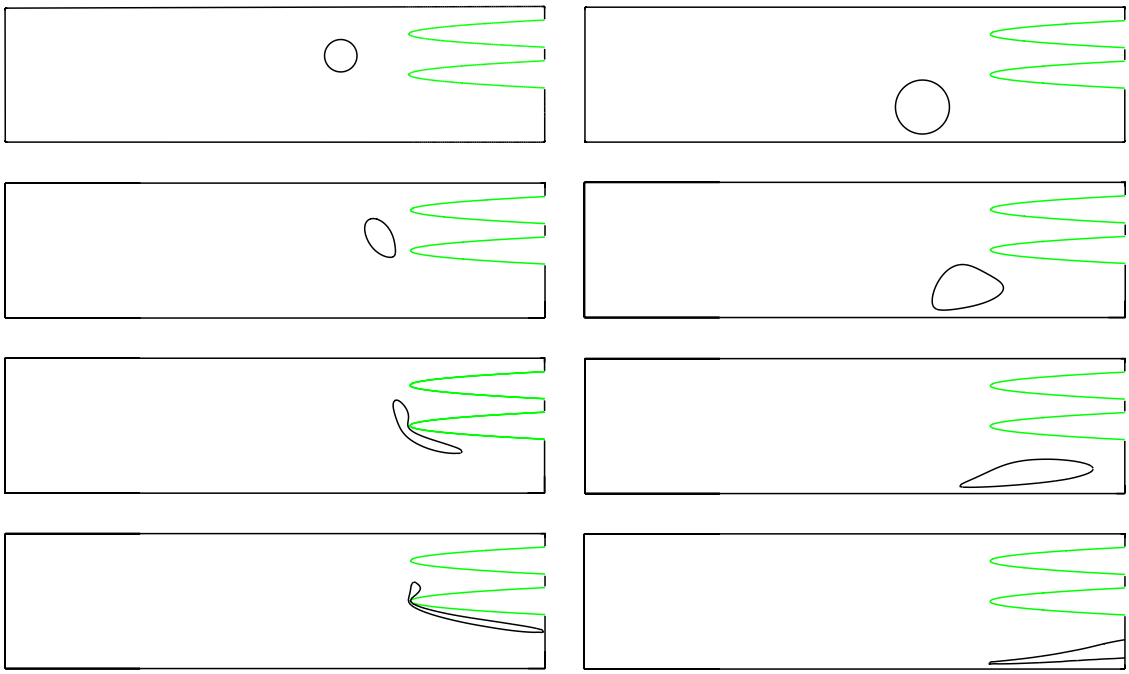

Fig. 4. Aiming to block a small daughter (left) and a larger daughter (right). The viscosity of both the glue and the blood is taken as unity. Shown from top to bottom at non-dimensional times 0, 2, 4 and 6.

to two daughters, have the viscosity of the glue being unity on the left and 10 on the right. The form of the divider starting at $x = 3$ is given by $(y - 0.5)^2 = (x - 3)/50$; hence the flow has symmetry about the line $y = 0.5$. Familiar shapes of the glue interface position occur [36] for the case $\rho = 1$ of present concern relatively far upstream of the branching, where an arrowhead-type shape is observed for the interface position, similar to those in [37]. The glue spreads into the two daughter vessels with a thin layer of glue becoming attached to the daughter walls and a propagating head which travels more freely into both daughters. At later times, the head proceeds out of the computational domain. The case where the viscosity ratio ν_1/ν_2 is raised to 10 is also shown in this figure. Similar flow characteristics are observed at small times, but the arrowhead-type shape seen when both fluids are of the same viscosity is now suppressed, and only a slight deviation to the back upstream side of the droplet is observed. Calculations at even higher viscosity ratio confirmed the trend. The droplet impinges on the daughter entrance at slightly later times than the first case, and a thicker layer of glue is observed adhering to the daughter wall. Notice here also that the head of the daughter is of a different shape from that observed for the single-fluid case.

Next, Fig. 3 shows the flow where there are four daughters, again with the glue injected in the centre of the feeding artery and the viscosity ratio $\nu = 1$. Again the arrowhead shape is found before the glue encounters the daughter vessels. When the glue reaches the daughters it first enters the middle two daughters only, where the flow rates are higher, and only at later times is a thin layer of glue observed on the walls of the upper and lower daughters, once the bulk of the glue has passed through the outlet. On the right-hand side of Fig. 3 the case where the flow is non-symmetric is considered, with one of the daughters being significantly larger than the other two. Here, the upstream part of the glue deforms as in the previous example, but now the glue approaches the largest daughter and a deformed arrowhead shape is found in the daughter tube also. These specific examples give a flavour of the dynamics of the injected fluid. We now move on in order to model blocking scenarios for certain simple flow domains.

3.2. Simple blocking strategies

Fig. 4 shows cases where blocking of daughters is attempted, specifically, on the left, blocking a small daughter, and, on the right, blocking a larger daughter vessel. In the first case, the glue veers towards the larger daughter and travels into a smaller daughter and remains at the mouth of that vessel, whereas the majority of the glue travels down the larger daughter, where the flow rate is greater. On the right, it is intended to block the larger bottom daughter. As can be seen from the figure, the droplet is distorted by the near-wall shear flow, similarly to that in [38]. As the flow rates are larger here, the glue passes freely through the outlet at $x = 4$ and, as the last plot shows, only approximately half of the channel is taken up with glue.

Clearly, in both situations, neither of the intended vessels ends up being blocked! Other calculations show that for a small daughter the glue must be injected as closely as possible to the mouth of the daughter. Fig. 5 shows two examples. On the left is the case where the viscosity is kept constant at unity. Now, with the glue injected closer to the bifurcation, the glue

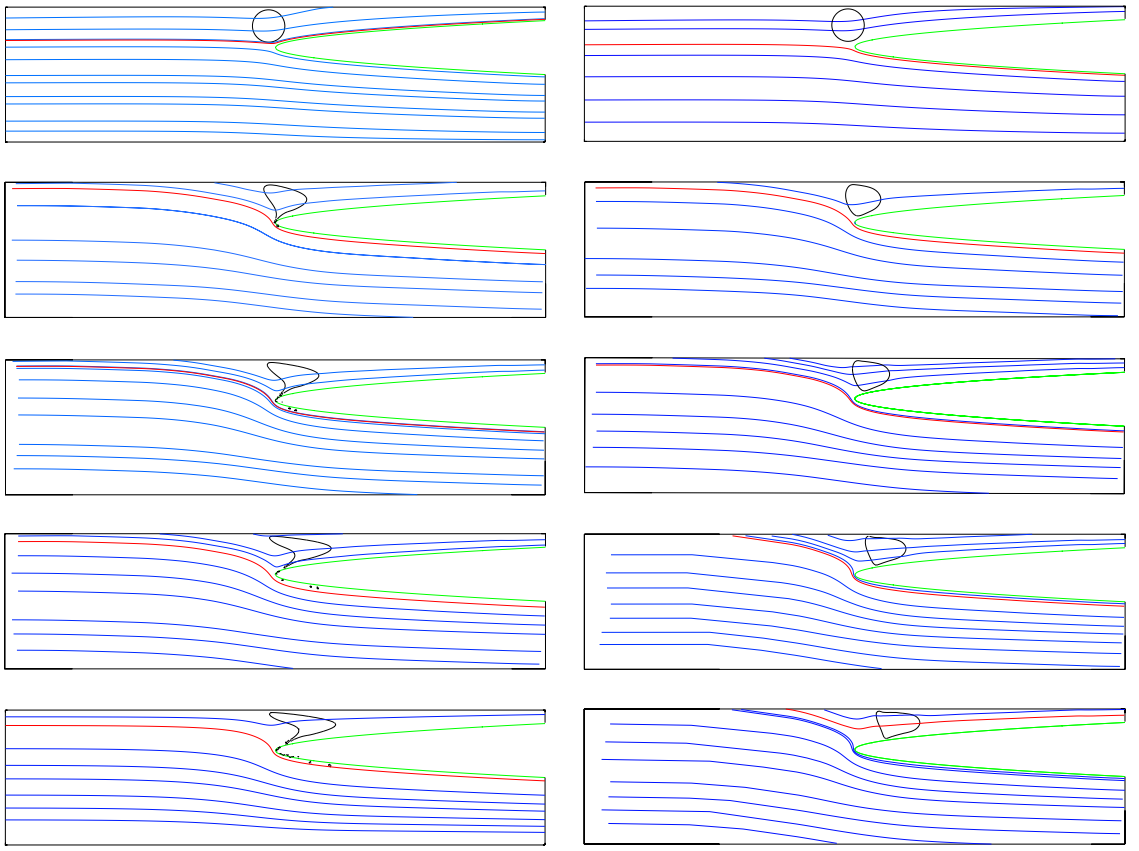

Fig. 5. Interface positions for the flow of an initially circular glue droplet from a single mother to two daughters. On the left, $\nu_1 = 1$, and right, $\nu_1 = e^{t/10}$, for non-dimensional times of 0, 5, 10, 15, and 20. For both cases, the dividing streamline is shown in red. (For interpretation of the references to colour in this figure legend, the reader is referred to the web version of this article.)

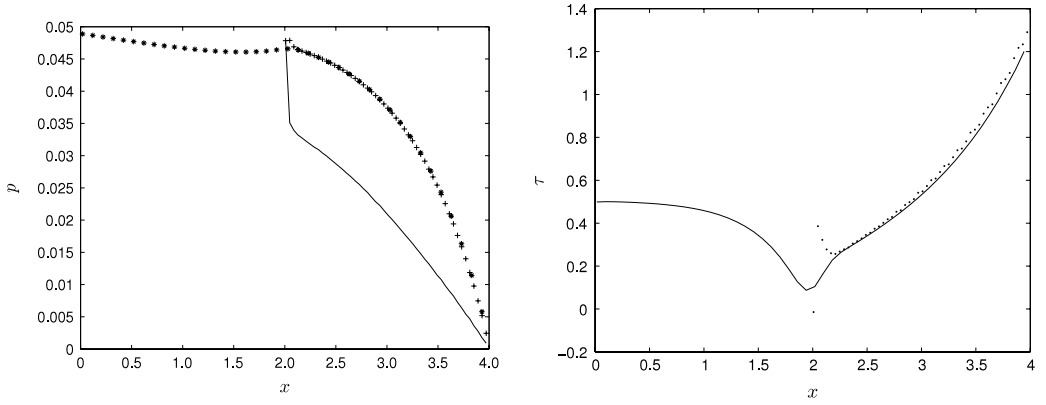

Fig. 6. Left: Pressure for the flow shown on the left of Fig. 5 where $\nu = 1$, at the upper mother wall, ($\star\star$) the upper daughter wall ($++$), and the lower daughter wall ($-$). Note the pressure jump at the entrance to the daughter vessel. Right: Wall shear at the top mother wall ($-$) and upper daughter wall ($\cdots$).

passes into the intended daughter, with the arrowhead shape being seen earlier in the mother vessel. Also, here, satellite droplets are ejected from the bulk of the glue and end up entering the larger daughter vessel. The glue takes up most of the daughter vessel, and in principle creates an effective barrier so that no blood can travel through the vessel; however, the satellite droplets of glue entering the larger daughter could have potentially damaging consequences, such as the onset of stroke. The right-hand side of Fig. 5 shows the case where the viscosity of the glue is allowed to vary with time, which is perhaps a more realistic model of the embolization process. We chose the form $\nu_1 = \exp(t/10)$, so that the glue initially is of the same viscosity as the blood, but then the glue viscosity rises to a value of e^2 at $t = 20$, as if solidifying. There is very little data available on polymerization time, but practice indicates that the polymerization time scale is such that solidification or

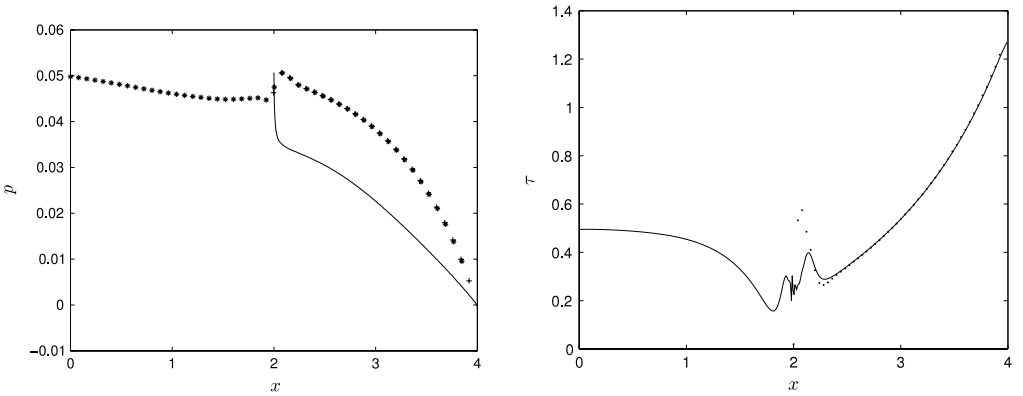

Fig. 7. Left: Pressure for the flow shown on the right of Fig. 5, where $\nu = e^{t/10}$, at the upper mother wall, ($\star\star$) the upper daughter wall ($++$), and the lower daughter wall ($-$). Note the pressure jump at the entrance to the daughter vessel. Right: Wall shear at the top mother wall ($-$) and upper daughter wall ($\cdots$).

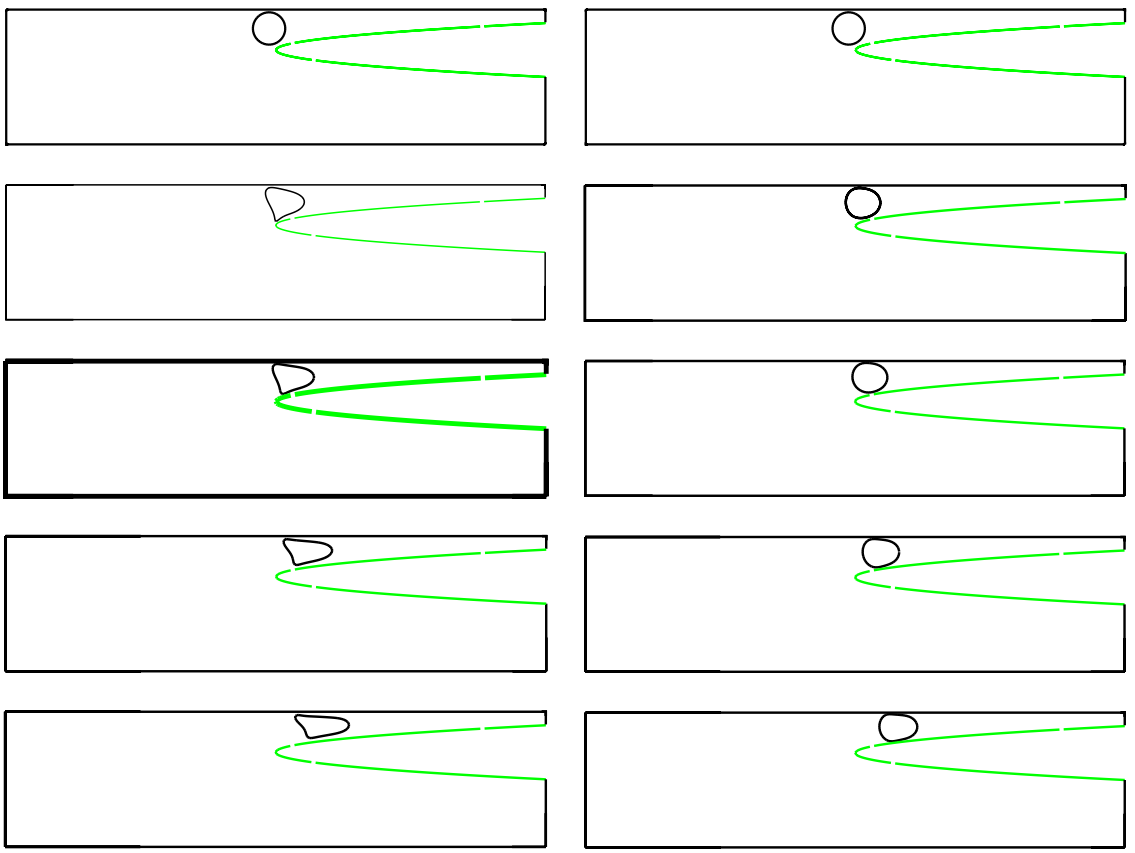

Fig. 8. Interface positions for the flow of an initially circular glue droplet from a single mother to two daughters. On the left, $We = 10\,000$; on the right, $We = 5000$.

stoppage takes place typically within the mother–daughter interaction regions, a feature which controls the choice of this functional form. In this case, the glue moves steadily into the daughter without any of the droplet breakup found previously. Also now, as the viscosity is larger, the arrowhead shape is not seen, and the droplet takes up most of the daughter channel. Moreover, as time progresses, the velocity of the glue is reduced, and as can be seen in the figure there is little motion taking place between the non-dimensional times $t = 15$ and 20.

Fig. 6 shows both the pressure and the wall shear for the case where $\nu = 1$. As indicated in Fig. 5(a), the streamlines seem to be approximately the same for all times after $t = 5$. In this steady-flow situation the results here can be compared to those in [12], where the flow in the presence of a near-wall branch is investigated. It is found in the latter work that there is in effect a pressure jump at an 'Euler zone', where the dynamics are inviscid to a close approximation, in the vicinity of the

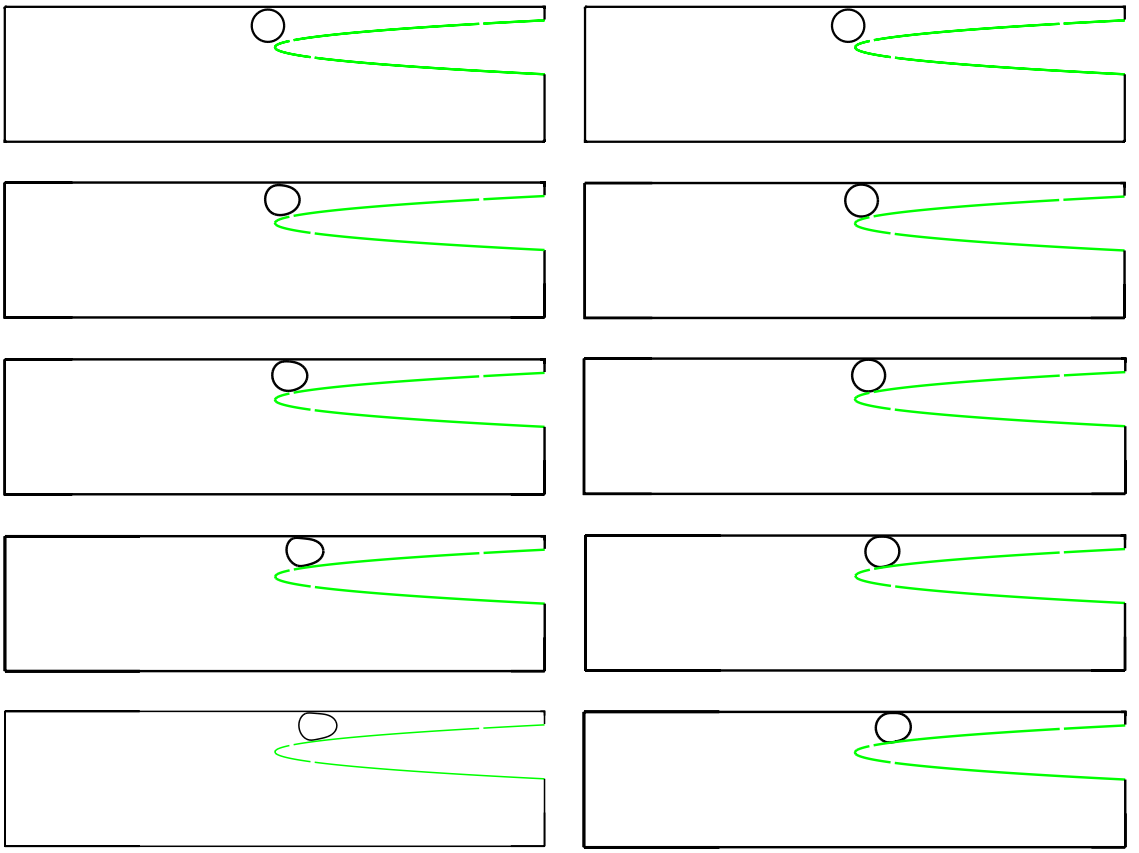

Fig. 9. Interface positions for the flow of an initially circular glue droplet from a single mother to two daughters. On the left, $We = 1000$; on the right, $We = 100$.

branching. Although in the case studied here the entrance to the daughter vessel may be outside the $O(\mathrm{Re}^{-1/3})$ thick wall layer of the feeding vessel, an effective jump in pressure can still be seen in this region. Fig. 6(b) shows the wall shear: as the flow seems almost steady, only one plot is shown, which corresponds to the shear for the mother and upper daughter walls at later times. It is observed that there is a decrease in shear on the mother wall until the flow reaches the small daughter. There is then a gradual increase but the overall wall shear remains low, representing a potentially important feature in the embolization process as high flow rates and hence high wall shear may damage the arterial wall. Also, significantly, no separation (flow reversal) is seen in either fluid in any of the flow configurations studied. As with the pressure, the wall shear in the daughter becomes very close to that of the continued mother vessel downstream.

The flow also becomes steady for the scenario where $\nu = e^{t/10}$. Fig. 7 shows the pressure and wall shear for this scenario. Similar features are seen here, with the effective pressure jump clearly evident, and the shear profiles at both the mother and upper daughter walls being very close to the $\nu = 1$ example, except at a small zone near the branching, where the viscosity of the glue is now larger. The value for the wall shear stress reaches a minimum before the branching starts, and once more no flow reversal is seen. The figure shows that the shear on the walls of both the continued mother and upper daughter are very close, which could be explained by the flow developing a lubrication-like nature downstream in the upper daughter vessel.

4. Effects of surface tension

To improve the model and simulate more realistic shapes of glue droplets, surface tension effects are now considered. The momentum and continuity equations remain the same, but the normal-stress condition at the interface is now replaced by

$$-p_1\mathbf{I} + 2\mu_1\mathbf{D}_1 \cdot \mathbf{n} = -p_2\mathbf{I} + 2\mu_2\mathbf{D}_2 \cdot \mathbf{n} + \sigma\kappa\mathbf{n}, \tag{12}$$

where σ is the surface tension coefficient and κ is the non-dimensional curvature of the glue/blood interface. The relevant non-dimensional parameter is the Weber number, given by $We = \rho U^2 L/\sigma$. A capillary number can be defined as $Ca = \mu U/\sigma$, so that $Ca = We/Re$. The same geometries and initial conditions as used for the scenario with no surface tension (We, $Ca \to \infty$) are considered here, so that direct comparisons can be made. As there is little data available for the surface tension coefficient σ, we present the results as a function of Weber number. The Reynolds number is again set to 400, but similar results were found with Reynolds numbers still over the range quoted earlier in the text.

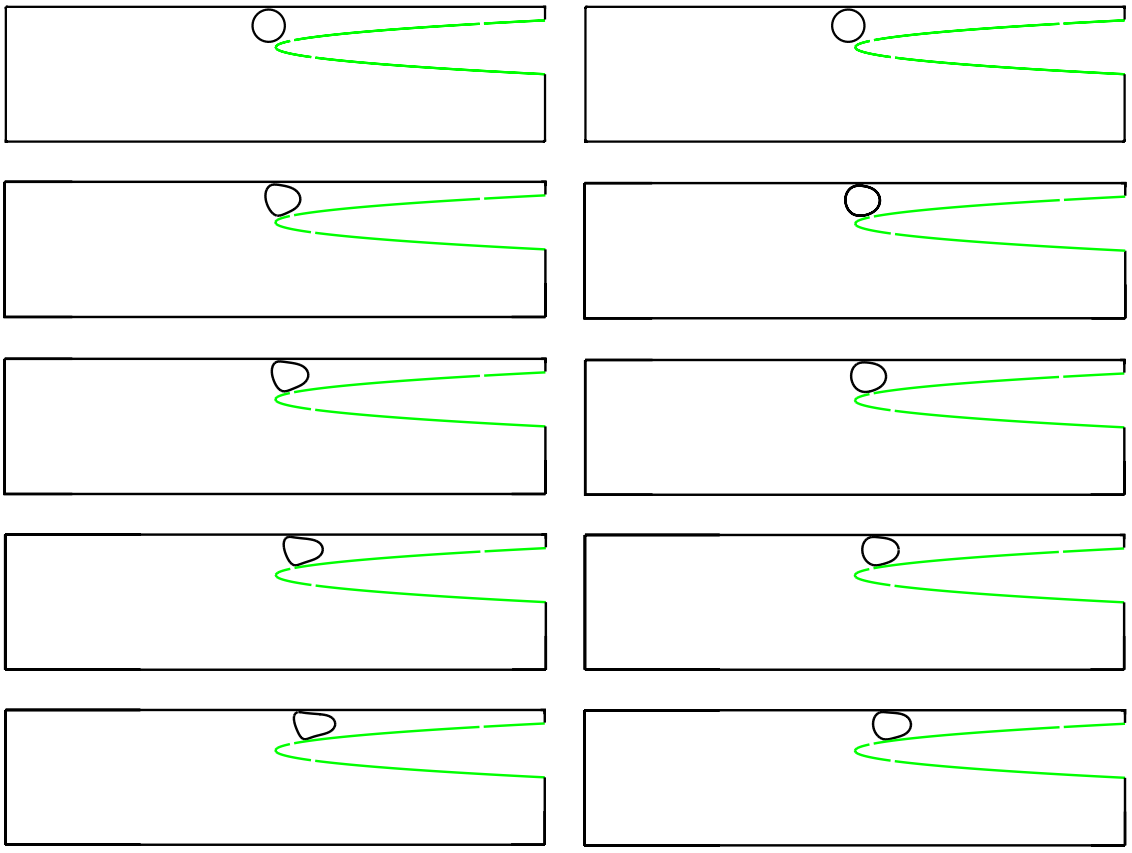

Fig. 10. Interface positions for the flow of an initially circular glue droplet from a single mother to two daughters. On the left, $We = 10\,000$; on the right, $We = 5000$. The viscosity is assumed to be of the form $\nu_1 = e^{t/10}$.

Results in Figs. 8–11 are presented for Weber numbers of 10 000, 5000, 1000, and 100. For the flows at Weber number 10 000, there is little difference in the results for interface shapes from the case where surface tension is neglected. As the Weber number is reduced and surface tension effects come more into play, the arrowhead shape seen in the limit of infinite Weber number disappears. For instance, in Fig. 9, for the Weber number of 5000, the upstream portion of the glue droplet retains its concave profile throughout the motion, a phenomenon also occurring at lower Weber numbers, as expected (see Fig. 9). As the Weber number is lowered, the shape of the droplet is less distorted from its original circular shape. Indeed, when the Weber number is 100, we see that the glue droplet is only slightly distorted, and moreover the droplet takes up most of the daughter channel at $t = 20$; there is little motion after this time. It would seem then that, in the simplified geometry modelled in Figs. 8 and 9, a flow with a Weber number of 100 is perhaps near the ideal in order for the glue to block the channel. In this case, the glue enters the daughter, does not travel too far into the daughter vessel, and then takes up the whole of the vessel.

Next, the effects of variable viscosity are again incorporated into the model. The same form of time-dependent viscosity as previously is chosen for the computations, results being presented in Figs. 10 and 11 for Weber numbers 10 000, 5000, 1000, and 100. For the case $We = 10\,000$ the resulting glue/blood interface position is seen to be quite different from the constant-viscosity case. When the viscosity is variable, the back of the glue droplet remains straight, and the droplet is less elongated in the streamwise direction. For smaller Weber numbers, it seems that the effects of variable viscosity are less important. The bottom figures on the right of Figs. 9 and 11, for instance, show that there is very little difference between the interface shapes for the cases of variable and constant viscosity flows. Although the modelling here is very simple, the above shows that the surface tension effect actually has a greater bearing on the dynamics in this simplified setting compared to the form of the time variation of the viscosity.

5. Discussion and further work

With the focus on the dynamics of two-phase flow, a basic computational model for the embolization process has been formulated in the present investigation. There appears to be no other such quantitative mathematical modelling predicting glue outputs for example as in Figs. 2–5. Although the approach may be simplistic in nature as regards the main application, the governing equations are still rich enough that a fully numerical technique is the most appropriate.

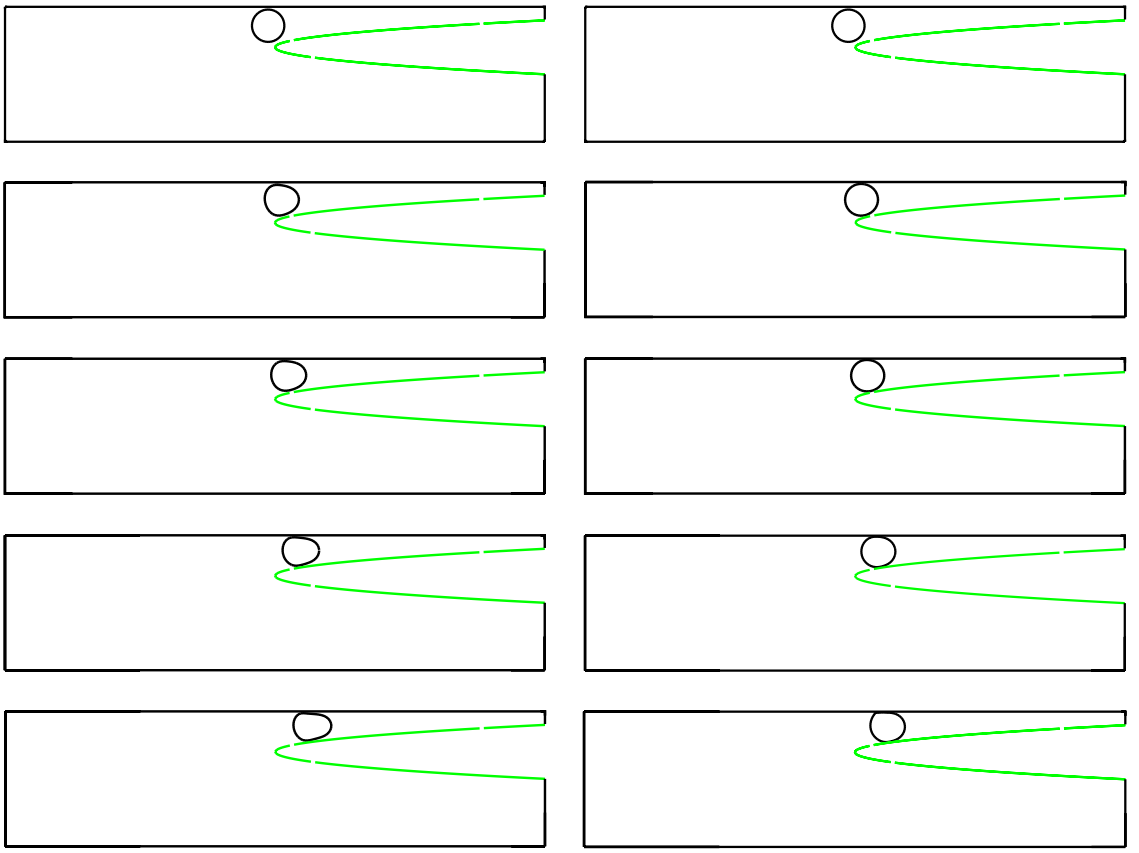

Fig. 11. Interface positions for the flow of an initially circular glue droplet from a single mother to two daughters. On the left, $We = 1000$; on the right, $We = 100$. The velocity is assumed to be of the form $v_1 = e^{t/10}$.

The flow to two, three, and four daughters was analysed with both symmetric and non-symmetric configurations of daughter shapes and droplet positions considered. The results have interesting repercussions. Granted that the model used in the current work is relatively simple, some tentative comments intended for medical practitioners may be relevant. When the density of the glue and the blood are nearly the same, it seems that injecting the glue close to the bifurcation is important if the artery to be embolized is smaller than neighbouring vessels. When the artery to be glued is larger, it seems less important to inject close to the bifurcation, as the front of the droplet travels towards the largest daughter. In this case however it would appear that the viscosity of the glue would need to be considerably larger than that in the cases where the blocking of a smaller daughter is attempted. The large viscosity of the glue is needed in effect to try to stop the glue passing through the vessel before it sets, due to the larger flow rates seen here.

Next, inclusion of surface tension forces leads to more realistic droplet shapes. Figs. 8–11 presented droplet shapes for Weber numbers in the range 100 to 10 000. Typically, for low Weber numbers, the droplet keeps its circular shapes and moves smoothly into the daughter vessel and takes up the whole of the channel width. Results for glues with variable viscosities show similar trends.

There are numerous extensions of the model that can make it more realistic. This is a relatively simple model for an extremely complicated neurosurgical process. Perhaps the first factor to consider in future work would be the non-Newtonian behaviour of the glue and the chemical reaction between the glue and the blood. Also, the assumption of the downstream pressures in all vessels being equal could be replaced with more practical values. The geometries considered in this work also are very simplified and could be extended, for instance to three dimensions, for pipe flow; compressibility effects also could be studied. Further, as a referee has pointed out, wall flexibility merits attention likewise, with allowance for passive and active responses. An ultimate goal would be patient-specific modelling. Although clearly this is a formidable challenge, consisting of problems in imaging, meshing, and computational fluid dynamics, the latter two are certainly tractable using the Gerris flow solver along with the gts meshing facility (http://gts.sourceforge.net), which has been demonstrated to work well with Gerris in very complicated three-dimensional geometries.

Acknowledgments

The authors would like to thank Mr N. Kitchen and Dr F. Robertson for their input regarding the neurosurgical application of this work and Dr Ann Taylor for providing Fig. 1. We would also like to thank Pierre-Yves Lagrée and Geordie McBain for

help implementing Gerris. The studentship for AHW from The Centre for Mathematics and Physics in the Life Sciences and Experimental Biology (CoMPLEX) at UCL is gratefully acknowledged as is the funding from EPSRC. The referees' helpful comments are much appreciated.

References

[1] R. Al-Shahi, J. Fang, S. Lewis, C. Warlow, Prevalence of adults with brain arteriovenous malformations: a community based study in Scotland using capture–recapture analysis, J. Neurol. Neurosurg. Psychiatry 73 (2002) 547–551.
[2] A. Lussenhop, W. Spence, Artificial embolization of cerebral arteries: report of use in a case of arteriovenous malformation, J. Amer. Medical. Assoc. 11 (1960) 1153–1155.
[3] L. Formaggia, D. Lamponi, A. Quarteroni, One-dimensional models for blood flow in arteries, J. Engrg. Math. 47 (2003) 251–276 (Mathematical modelling of the cardiovascular system).
[4] M.J. Lighthill, Physiological fluid dynamics: a survey, J. Fluid Mech. 52 (1972) 475–497.
[5] F. van de Vosse, Mathematical modelling of the cardiovascular system, J. Engrg. Math. 47 (2003) 175–183.
[6] K. Yokoi, F. Xiao, H. Liu, K. Fukasaku, Finite element simulation of blood flow in a realistic model of a moving human right coronary artery, in: Proceedings of The 10th Annual Conference of The CFD Society of Canada, J. Comput. Phys. 202 (2005) 317.
[7] E. Lo, J. Fabrikant, R. Levy, M. Phillips, K. Frankel, E. Alpen, An experimental compartmental flow model for assessing the hemodynamic response of intracranial arteriovenous malformations to stereotactic radiosurgery, Neurosurgery 28 (1991) 251.
[8] G.J. Hademenos, T. Massoud, F. Vinuela, A biomathematical model of intrecranial malformations based on electrical circuit network analysis, Neurosurgery 38 (1996) 1345–1358.
[9] R.I. Bowles, S.C.R. Dennis, R. Purvis, F.T. Smith, Multi-branching flows from one mother tube to many daughters or to a network, Philos. Trans. R. Soc. A. 363 (2005) 1045–1055.
[10] F.T. Smith, M.A. Jones, One-to-few and one-to-many branching tube flows, J. Fluid Mech. 423 (2000) 1–31.
[11] F.T. Smith, M.A. Jones, AVM modelling by multi-branching tube flow: large flow rates and dual solutions, Math. Med. Biol. 20 (2003) 183–204.
[12] F.T. Smith, N.C. Ovenden, P.T. Franke, D. Doorly, What happens to pressure when a flow enters a side branch? J. Fluid Mech. 479 (2003) 231–258.
[13] M.G. Blyth, A.J. Mestel, Steady flow in a dividing pipe, J. Fluid Mech. 401 (1999) 339–364.
[14] M. Tadjfar, F.T. Smith, Direct simulations and modelling of basic three-dimensional bifurcating tube flows, J. Fluid Mech. 519 (2004) 1–32.
[15] T. Pedley, Mathematical modelling of arterial fluid dynamics, J. Engrg. Math. 47 (2003) 419–444.
[16] M. Mazzeo, P. Coveney, HemelB: A high performance parallel lattice-boltzmann code for large scale fluid flow in complex geometries, Comput. Phys. Comm. 178 (2008).
[17] N.C. Ovenden, F.T. Smith, G.X. Wu, The effects of nonsymmetry in a branching flow network, J. Engrg. Math. 63 (2009) 213–239.
[18] J.B. Grotberg, O. Jensen, Biofluid mechanics in flexible tubes, Annu. Rev. Fluid Mech. 36 (2004) 121–147.
[19] J.E.F. Green, N.C. Ovenden, F.T. Smith, Models of motion of a single fluid through a branched network with moving walls, J. Engrg. Math. 64 (2009) 353–365.
[20] M. Yaşargil, Avm of the Brain: Clinical Considerations, General and Special Operative Techniques, Surgical Results, Nonoperated Cases, Cavernous and Venous Angiomas, Neuroanesthesia, Vol. 3, George Thieme Verlag, 1988.
[21] A.H. White, F.T. Smith, Wall shape effects on multiphase flow in channels, Theoret. and Comp. Fluid Dynamics (2012) 1–22.
[22] R. Scardovelli, S. Zaleski, Direct numerical simulation of interfacial flow, Annu. Rev. Fluid Mech. 31 (1999) 567–603.
[23] C.W. Hirt, B.D. Nichols, Volume of Fluid (VOF) method for dynamics of free boundaries, J. Comput. Phys. 39 (1981) 201–225.
[24] D. Gueyffier, J. Li, A. Nadim, R. Scardovelli, S. Zaleski, Volume of Fluid interface tracking with smoothed surface stress methods for three-dimensional flows, J. Comput. Phys. 152 (1999) 423–456.
[25] E. Aulisa, S. Manservisi, R. Scardovelli, S. Zaleski, Interface reconstruction with least-squares fit and split advection in three-dimensional Cartesian geometry, J. Comput. Phys. 225 (2007) 2301–2319.
[26] A. Prosperetti, G. Tryggvason, Computational Methods for Multiphase Flow, Cambridge Univ Pr., 2007.
[27] A.J. Chorin, Numerical solution of the Navier–Stokes equations, Math. Comp. 22 (1968) 745–762.
[28] S. Popinet, Gerris: a tree-based adaptive solver for the incompressible Euler equations in complex geometries, J. Comput. Phys. 484 (2003) 69–83.
[29] J.B. Bell, P. Colella, H.M. Glaz, A second-order projection method for the incompressible Navier–Stokes equations, J. Comput. Phys. 85 (1989) 257–283.
[30] J. Howington, C. Kerberb, L. Gutermana, L. Hopkins, Liquid embolic agents in the treatment of intracranial arteriovenous malformations, Neurosurg. Clin. N. Am. 17 (2005) 135–147.
[31] S. Afkhami, A. Leshansky, Y. Renardy, Numerical investigation of elongated drops in a microfluidic T-junction, Phys. Fluids 23 (2011) 2002.
[32] C. Chung, M. Lee, K. Char, K. Ahn, S. Lee, Droplet dynamics passing through obstructions in confined microchannel flow, Microfluid. Nanofluid. 9 (2010) 1151–1163.
[33] A. Carlson, M. Do-Quang, G. Amberg, Droplet dynamics in a bifurcating channel, Int. J. of Multiphase Flow 36 (2010) 397–405.
[34] A.H. White, Mathematical modelling of the embolization process for the treatment of arteriovenous malformations, Ph.D. Thesis, University of London, 2008, p. 329.
[35] J. Stark, M. Manga, The motion of long bubbles in a network of tubes, Transp. Porous Media 40 (2000) 201–218.
[36] L. Chen, S. Garimella, J. Reizes, E. Leonardi, The development of a bubble rising in a viscous liquid, J. Fluid Mech. 387 (1999) 61–96.
[37] D. Lorstad, L. Fuchs, High-order surface tension vof-model for 3d bubble flows with high density ratio, J. Comput. Phys. 200 (2004) 153–176.
[38] J. Li, Y. Renardy, M. Renardy, Numerical simulation of breakup of a viscous drop in simple shear flow through a volume-of-fluid method, Phys. Fluids 12 (2000) 269.